Near-field polarization of a high-refractive-index dielectric nanosphere on a dielectric substrate

Yu. V. Vladimirova,[1,2,3,*] V. G. Arakcheev,[1] F. Song,[5] and V. N. Zadkov[3,4]

[1]*Department of Physics and International Laser Center, Lomonosov Moscow State University, Moscow 119991, Russia*

[2]*Quantum Technology Center, Lomonosov Moscow State University, Moscow 119991, Russia*

[3]*Faculty of Physics, Higher School of Economics, Old Basmannya 21/4, Moscow, Russia*

[4]*Institute of Spectroscopy Russian Academy of Sciences, Troitsk, Moscow 108840, Russia*

[5]*College of Physical Sciences, Nankai University, Tianjin 300071, People's Republic of China*

(Received 8 July 2019; published 28 August 2019)

The near-field polarization structure of a high-refractive-index dielectric nanosphere in a nonmagnetic and nonabsorbing medium is studied numerically in free space and in the vicinity of a flat dielectric substrate. Polarization patterns of the near field are obtained for linear and circular polarizations of the incident light and visualized using the polarization degree and three-dimensional Stokes parameters. Calculations are performed using the finite-element method and verified analytically using the Mie solution for scattering by a sphere with an extension of Weyl's method allowing description of reflection by a flat substrate. It is shown that the nanosphere drastically affects the polarization leading to a complex butterflylike structure. For instance, the near-field polarization is found to be qualitatively modified near the Mie electric and magnetic dipole and quadrupole resonances: linear polarization of the incident field results in circular polarization in some areas around the particle and vice versa. The areas of strong polarization change are found to be spatially localized in certain places around the particle making it possible to perform an experimental mapping. It is shown how a dielectric substrate affects the polarization distribution of the near-field of the particle. Also, several schemes of potential experiments to map the near-field intensity and polarization have been discussed.

DOI: 10.1103/PhysRevA.100.023847

I. INTRODUCTION

Interaction of light with nanoparticles whose size is much smaller than the light wavelength has been studied in detail for the last few decades, forming the whole field of nanophotonics, nanoplasmonics inclusive [1–6]. It has been demonstrated that both metal and dielectric nanoparticles provide the whole bunch of possibilities to essentially control the near-field and the directivity pattern of the scattered light. It has also been shown that a nanoparticle can drastically affect the decay rates of the quantum emitters (atoms, molecules, or quantum dots), referred to as the Purcell effect [7], providing a way to control the processes of their emission, scattering, and absorption. Plasmonic and dielectric nanoparticles have been a subject of a vast number of theoretical and experimental works considering different aspects of the problem: various size and geometry, the material the nanoparticles are made of, and the influence of the environment on the near-field intensity [8–11]. The polarization patterns of the near field, however, have been considered only recently for the plasmonic nanoparticles [12–15] and nanostructures [16,17], and have been found to be essentially complex, regardless of the incident light polarization for nanoparticles both in free space [12,13] and in the vicinity of a dielectric substrate [14], which is of great importance for such applications as the near-field microscopy [18], photovoltaic cells with embedded plasmonic nanoparticles [19], surface-enhanced Raman scattering [20], and polarization-sensitive tip-enhanced Raman scattering [21–25].

In recent years, the dielectric nanoparticles with high-refractive-index started to attract more attention as they have small ohmic losses [6,26,27] and, thus, show greater potential for controlling the near field and the scattered radiation pattern by exciting the electric and magnetic multipoles in the particle. In particular, strongly directed scattering patterns can be achieved by tuning the parameters of the dielectric nanoparticle [28,29]. In addition to the near-field intensity, the polarization pattern of the near field also plays an important role in the interaction of a quantum emitter with the near field, though being much less acknowledged and studied. For instance, polarization control allows both selective excitation of the specific quantum transitions in a quantum emitter and control of its fluorescence intensity [30,31].

In this paper, we analyze in detail the near-field polarization pattern of a high-refractive-index spherical nanoparticle in a nonmagnetic and nonabsorbing medium both in free space and in the vicinity of a flat dielectric substrate. Two types of incident light polarization are considered: linear and circular. Calculations are performed both numerically using the finite-element method (COMSOL Multiphysics package) and analytically using the Mie solution for scattering by a sphere. The analytical approach also uses an extension of Weyl's method to calculate reflection of dipole radiation by a flat substrate. The results obtained using the two approaches are compared in order to analyze the applicability of the numerical approach for more complicated cases, which can be hardly described analytically.

*yu.vladimirova@physics.msu.ru

II. SCATTERING BY A SPHERE NEAR A DIELECTRIC SUBSTRATE

In this section, we derive an analytical solution for the near field of a single spherical dielectric nanoparticle placed near a flat dielectric substrate that is irradiated by an incident plane electromagnetic wave.

Let us assume that a particle of radius r is placed in a nonabsorbing and nonmagnetic medium ($\mu = \mu_{\text{media}} = \mu_{\text{subs}} = 1$) at the distance h from the substrate surface. Then, for a plane incident electromagnetic wave, the near field of the particle in free space can be calculated using the solutions obtained by Mie [32] and Debye [33]. To describe the reflection from a flat substrate, it is convenient to use the Weyl's method [34] for a single spherical wave [35], which can be generalized for a series of spherical waves [36]. Let us consider a formal solution for the field W^S scattered by the nanosphere placed above the substrate following the concept developed previously [36,37]. Let V^I and V^R be the incident and reflected (from the substrate) plane waves, respectively, linked by the Fresnel equations. The field W^S is also reflected from the substrate inducing a field V^{SR}:

$$V^{SR} = \hat{\mathbf{A}} \cdot W^S, \tag{1}$$

where the matrix $\hat{\mathbf{A}}$ describes the reflection of spherical waves by the substrate. On the other hand, the currents flowing in the nanosphere, resulting in W^S, are caused by all three fields V^I, V^R, and V^{SR}, so that the general equation for the scattered field can be written as follows:

$$W^S = \hat{\mathbf{B}} \cdot (V^I + V^R + V^{SR}),$$

where $\hat{\mathbf{B}}$ is a well-known matrix of the Mie scattering coefficients [38]. Thus, the general equation for the scattered field can be written in the following form:

$$W^S = (\mathbf{1} - \hat{\mathbf{B}} \cdot \hat{\mathbf{A}})^{-1} \cdot \hat{\mathbf{B}} \cdot (V^I + V^R). \tag{2}$$

The elements of the reflection matrix $\hat{\mathbf{A}}$ contain the Weyl's type integrals and are expressed in the form [36]

$$A_{l',m';l,m} = i^{l'-1}\sqrt{\frac{2l'+1}{l'(l'+1)}}(-1)^{m-1}\delta_{mm'}\int_0^{\pi/2-i\infty} d\alpha \sin\alpha\, e^{2iq\cos\alpha}\, a^m_{l',f';l,f},$$

where

$$\begin{aligned}
a^m_{l',e;l,e}(\alpha) &= r_p(\cos\alpha)\widetilde{V}^m_l(\cos\alpha)d^{l'}_{m,-}(\pi-\alpha) + r_s(\cos\alpha)\widetilde{U}^m_l(\cos\alpha)d^{l'}_{m,+}(\pi-\alpha),\\
a^m_{l',h;l,e}(\alpha) &= -i\big\{r_p(\cos\alpha)\widetilde{V}^m_l(\cos\alpha)d^{l'}_{m,+}(\pi-\alpha) + r_s(\cos\alpha)\widetilde{U}^m_l(\cos\alpha)d^{l'}_{m,-}(\pi-\alpha)\big\},\\
a^m_{l',e;l,h}(\alpha) &= i\big\{r_p(\cos\alpha)\widetilde{U}^m_l(\cos\alpha)d^{l'}_{m,-}(\pi-\alpha) + r_s(\cos\alpha)\widetilde{V}^m_l(\cos\alpha)d^{l'}_{m,+}(\pi-\alpha)\big\},\\
a^m_{l',h;l,h}(\alpha) &= r_p(\cos\alpha)\widetilde{U}^m_l(\cos\alpha)d^{l'}_{m,+}(\pi-\alpha) + r_s(\cos\alpha)\widetilde{V}^m_l(\cos\alpha)d^{l'}_{m,-}(\pi-\alpha),
\end{aligned} \tag{3}$$

and the functions $r_p(\cos\alpha)$ and $r_s(\cos\alpha)$ represent the Fresnel reflection coefficients for the parallel and perpendicular polarizations, respectively, and

$$\begin{aligned}
\widetilde{U}^m_l = {} & i^{1-l}\frac{l-1}{2}\left\{\sqrt{\frac{(l+m-1)(l+m)}{(2l-1)(2l+1)}}\widetilde{P}^{m-1}_{l-1} - \sqrt{\frac{(l-m-1)(l-m)}{(2l+1)(2l-1)}}\widetilde{P}^{m+1}_{l+1}\right\}\\
& - i^{-1-l}\frac{l+2}{2}\left\{\sqrt{\frac{(l-m+1)(l+m+2)}{(2l+3)(2l+1)}}\widetilde{P}^{m-1}_{l-1} + \sqrt{\frac{(l-m+1)(l+m+2)}{(2l+3)(2l+1)}}\widetilde{P}^{m+1}_{l+1}\right\},
\end{aligned}$$

$$\widetilde{V}^m_l = \frac{1}{2}i^{1-l}\big\{\sqrt{(l-m+1)(l+m)}\widetilde{P}^{m-1}_l - \sqrt{(l+m+1)(l-m)}\widetilde{P}^{m+1}_l\big\},$$

where

$$\widetilde{P}^m_l(\cos\alpha) = \sqrt{(2l+1)\frac{(l-m)!}{(l+m)!}}P^m_l(\cos\alpha)$$

is the normalized Legendre function with

$$\begin{aligned}
d^{l'}_{m,-}(\pi-\alpha) &= \tfrac{1}{2}\big\{d^{l'}_{m,1}(\pi-\alpha) - d^{l'}_{m,-1}(\pi-\alpha)\big\},\\
d^{l'}_{m,+}(\pi-\alpha) &= \tfrac{1}{2}\big\{d^{l'}_{m,1}(\pi-\alpha) + d^{l'}_{m,-1}(\pi-\alpha)\big\},
\end{aligned} \tag{4}$$

where "+" and "−" indicate the symmetrical and antisymmetrical combinations of the function $d^l_{m,m'}(\alpha)$ defined as

$$d^l_{m,m'}(\alpha) \equiv \sqrt{(l+m')!(l-m')!(l+m)!(l-m)!}\sum_k (-1)^k \frac{\left(\cos\frac{\alpha}{2}\right)^{2l+m'-m-2k}\left(\sin\frac{\alpha}{2}\right)^{m-m'+2k}}{(l-m-k)!(l+m'-k)!(k+m-m')!k!}.$$

The total field (**E**, **H**) represents a sum of contributions of the incident, reflected, and scattered fields V^I, V^R, V^{SR}, and W^S and can be expressed using the Debye potentials in the form

$$\mathbf{E} = \nabla\times\nabla\times(\mathbf{r}^e D) + ik\nabla\times(\mathbf{r}^h D), \quad \mathbf{H} = \sqrt{\varepsilon_m}\nabla\times\nabla\times(\mathbf{r}^h D) - ik\nabla\times(\mathbf{r}^e D),$$

where the Debye potentials include contributions of the four fields represented by the expansions [39]

$$\begin{aligned} {}^eD(r) &= \sum_{l=1}^{\infty}\sum_{m=-l}^{l}\left[\left({}^e\nu_l^{m\,I} + {}^e\nu_l^{m\,R} + {}^e\nu_l^{m\,SR}\right)\Psi_l^m(r) + {}^e w_l^{m\,S}\,\Pi_l^m(r)\right], \\ {}^hD(r) &= \sum_{l=1}^{\infty}\sum_{m=-l}^{l}\left[\left({}^h\nu_l^{m\,I} + {}^h\nu_l^{m\,R} + {}^h\nu_l^{m\,SR}\right)\Psi_l^m(r) + {}^h w_l^{m\,S}\,\Pi_l^m(r)\right], \end{aligned} \tag{5}$$

where

$$\Psi_l^m = j_l(kr)Y_l^m(\vartheta,\phi), \quad \Pi_l^m = h_l^{(1)}(kr)Y_l^m(\vartheta,\phi),$$
$$Y_l^m(\vartheta,\phi) = \left[(2l+1)\frac{(l-m)!}{(l+m)!}\right]^{1/2} P_l^m(\cos\vartheta)e^{im\phi},$$

and $j_l(\rho)$, $h_l^{(1)}(\rho)$, and $P_l^m(\cos\vartheta)$ are the spherical Bessel and Hankel functions and the Legendre polynomials, respectively. For the *p*-polarized incident wave, the elements of the vectors V^I and V^R are expressed as [37]

$${}^e\nu_l^{mI} = \frac{i^{l-1}}{k}\sqrt{\frac{2l+1}{l(l+1)}}(-1)^{m-1}d^l_{m,-}(\theta_i), \quad {}^h\nu_l^{m\,I} = -\frac{i^l}{k}\sqrt{\frac{2l+1}{l(l+1)}}(-1)^{m-1}d^l_{m,+}(\theta_i),$$
$${}^e\nu_l^{m\,R} = \frac{i^{l-1}}{k}e^{2iq\cos\vartheta_i}r_p(\cos\theta_i)\sqrt{\frac{2l+1}{l(l+1)}}(-1)^l d^l_{m,-}(\theta_i),$$
$${}^h\nu_l^{m\,R} = -\frac{i^l}{k}e^{2iq\cos\vartheta_i}r_p(\cos\theta_i)\sqrt{\frac{2l+1}{l(l+1)}}(-1)^{l-1}d^l_{m,+}(\theta_i),$$

and for the *s*-polarized incident wave

$${}^e\nu_l^{m\mathrm{I}} = -\frac{i^l}{k}\sqrt{\frac{2l+1}{l(l+1)}}(-1)^{m-1}d^l_{m,+}(\theta_i), \quad {}^h\nu_l^{m\,\mathrm{I}} = -\frac{i^{l+1}}{k}\sqrt{\frac{2l+1}{l(l+1)}}(-1)^{m-1}d^l_{m,-}(\theta_i),$$
$${}^e\nu_l^{m\,R} = -\frac{i^l}{k}e^{2iq\cos\vartheta_i}r_s(\cos\theta_i)\sqrt{\frac{2l+1}{l(l+1)}}(-1)^{l-1}d^l_{m,+}(\theta_i),$$
$${}^h\nu_l^{m\,R} = \frac{i^{l+1}}{k}e^{2iq\cos\vartheta_i}r_s(\cos\theta_i)\sqrt{\frac{2l+1}{l(l+1)}}(-1)^l d^l_{m,-}(\theta_i),$$

where θ_i is the angle of incidence and the wave vector **k** of the incident wave is assumed to lie in the plane *yz*. The elements ${}^e w_l^{m\,S}$ and ${}^h w_l^{m\,S}$ of the vector W^S can be found from Eq. (2) by using the expansions of vectors V^I and V^R. Then the elements ${}^e\nu_l^{m\,SR}$ and ${}^h\nu_l^{m\,SR}$ of the vector V^{SR} are similarly obtained from Eq. (1).

As a result, the presented approach shows a systematic procedure for calculating the scattered field of irradiated dielectric particle placed above the dielectric flat substrate. The field is represented as an expansion in spherical coordinates. The polarization pattern of the particle's near field can be appropriately analyzed after transforming the result into Cartesian coordinates.

Polarization of the near field

The analysis of the near-field polarization distribution can be carried out in terms of the polarization degree and the generalized three-dimensional Stokes parameters [40]. The vector $\mathbf{E}(\mathbf{r})$ describes an ellipse with the semiaxes $E_{\min}$ and $E_{\max}$, so that for $\vec{E}_{\min} = 0$ the near field is linearly polarized, and for $E_{\min} = E_{\max}$ it is circularly polarized. The polarization

degree then is defined as

$$P = \frac{I_{\max} - I_{\min}}{I_{\max} + I_{\min}}, \tag{6}$$

where $P = 1$ corresponds to the linear and $P = 0$ to the circular polarization, respectively.

It is important to note that the polarization degree does not carry information about both the orientation of the polarization ellipse and the direction of the rotation of the vector $\mathbf{E}(\mathbf{r})$. For a complete description, it is convenient to use a set of the generalized three-dimensional Stokes parameters:

$$\begin{aligned}
&\Lambda_0 = \phi_{xx} + \phi_{yy} + \phi_{zz}, \quad \Lambda_1 = 3/2(\phi_{xy} + \phi_{yx}),\\
&\Lambda_2 = 3i/2(\phi_{xy} - \phi_{yx}), \quad \Lambda_3 = 3/2(\phi_{xx} - \phi_{yy}),\\
&\Lambda_4 = 3/2(\phi_{xz} + \phi_{zx}), \quad \Lambda_5 = 3i/2(\phi_{xz} - \phi_{zx}),\\
&\Lambda_6 = 3/2(\phi_{yz} + \phi_{zy}), \quad \Lambda_7 = 3i/2(\phi_{yz} - \phi_{zy}),\\
&\Lambda_8 = \sqrt{3}/2(\phi_{xx} + \phi_{yy} - 2\phi_{zz}),
\end{aligned}$$

where $\phi_{ij}(\mathbf{r}, \omega) = \langle E_i^*(\mathbf{r}, \omega) E_j(\mathbf{r}, \omega) \rangle$ and $i, j = x, y, z$ are the components of the spectral-density tensor and the symbol $\langle\,\rangle$ denotes the averaging over time. Similar to S_0 used in two-dimensional (2D) formalism, the first Stokes parameter Λ_0 is proportional to the total spectral density of the field. The pair of the parameters (Λ_1, Λ_2) play a role analogous to that of (S_2, S_3) in the 2D formalism, in which S_2 describes the excess in spectral density of the $+45^\circ$ linearly polarized component over the -45° linearly polarized component and S_3 describes the excess of the right-hand circularly polarized component over the left-hand circularly polarized component in the xy plane [38]. The pairs (Λ_4, Λ_5) and (Λ_6, Λ_7) play similar roles in the xz and yz planes, respectively. The parameter Λ_3 is analogous to S_1 and describes the excess of the x component over the y one. The component Λ_8 represents the sum of the excesses in spectral density in the x and y directions over that in the z direction. By analogy with the 3D Poincaré sphere for the 2D formalism, the polarization state of the 3D electromagnetic field can be characterized in terms of an 8D sphere.

III. NEAR-FIELD POLARIZATION PATTERN OF A DIELECTRIC NANOSPHERE IN FREE SPACE

In the following, we will consider a nanosphere made of silicon, which is chosen as an example of a high-refractive-index dielectric material that allows, by contrast with a metal, excitation of both electric and magnetic multipoles in the nanoparticle and interference between them, essentially enriching the near-field pattern. In addition, silicon is a widespread high-refractive-index dielectric material widely used in nanophotonics. For numerical calculations of the polarization patterns of the near field we will consider a nanosphere of 90 nm radius in free space ($\varepsilon_m = 1$), which is irradiated by a plane electromagnetic wave propagating along the z axis. The electric-field vector is directed along the y axis in the case of linear polarization of the incident wave or oscillates in the xy plane in the case of a circular polarized incident wave [Fig. 1(b)]. The Mie expansion can be used to derive expressions for the absorption, scattering, and extinction cross sections in terms of the coefficients a_n and b_n, which describe the electric and magnetic modes, respectively, so that the coefficients a_1 and b_1 correspond to the electric and magnetic dipole modes (ED and MD, respectively), a_2 and b_2 correspond to the electric and magnetic quadrupole modes (EQ and MQ, respectively), etc. Our estimations show that the contributions of the higher-order modes are negligible, even at the resonant frequencies, by contrast with the dipole mode quadrupole contributions, so that for simplicity we will consider from now on only the first two terms.

A high refractive index of silicon [Fig. 1(a)] causes corresponding sharp resonant peaks in the extinction spectrum of the nanosphere [Fig. 1(c)] in the wavelength range of $\lambda > 400$ nm at which the silicon extinction coefficient is low [Fig. 1(a)]. The peaks are significantly shifted from each other making it possible to excite a separate mode or a combination of modes by choosing the wavelength of the incident light. Hereafter, we focus on the four key wavelengths at which the maxima are observed: 580 nm (ED contribution, size parameter $q = 2\pi R/\lambda = 0.97$), 710 nm (MD contribution, $q = 0.79$), 470 nm (EQ contribution, $q = 1.2$), and 540 nm (MQ contribution, $q = 1.04$).

First, we consider a 3D distribution of the polarization degree for the case of the resonant irradiation at $\lambda = 710$ nm. The patterns calculated numerically using FEM [Figs. 2(a) and 2(b)] clearly show that the nanosphere drastically affects the polarization of the electric field resulting in a nontrivial and complex distribution in its vicinity and changing qualitatively the polarization. For instance, the linear polarization of the incident light leads to four large separate areas of elliptical polarization near the particle, which are represented by yellow 3D isosurfaces for $P = 0.6$ [Fig. 2(a)]. More clearly it is seen using the cross sections by three mutually orthogonal planes that pass through the areas of strong polarization change. Obtained distributions of the polarization degree, shifted from their exact place to the side planes of the graph, demonstrate that almost circular polarization with $P = 0.05$ (blue areas) is achieved inside two of the four areas of elliptical polarization in the close vicinity of the nanosphere [Fig. 2(a)]. Note that only the yz plane passes through the center of the sphere whereas the other two are shifted by more than the particle radius, i.e., they do not cross the particle.

The pattern of the polarization degree for the circularly polarized incident field [Fig. 2(b)], though essentially different from that considered above, also demonstrates similar qualitative change of the near-field polarization type: the polarization switches to almost linear in a large single area around the particle equator which is represented in Fig. 2(b) by a red isosurface with $P = 0.8$. Three mutually orthogonal cross sections, two of which pass through the center of the nanosphere, show that the area of polarization change resembles a toroid, whose axis coincides with z. In close vicinity of the nanosphere the polarization is almost linear, $P = 0.98$ [red areas in the two side cross sections in the Fig. 2(b)]. Thus, the obtained 2D and 3D distributions of the polarization degree show that the polarization switches from linear to circular (or vice versa) in certain areas in the vicinity of the dielectric nanosphere.

This nontrivial result has also been confirmed by analytical Mie calculations for a sphere in free space and the polarization

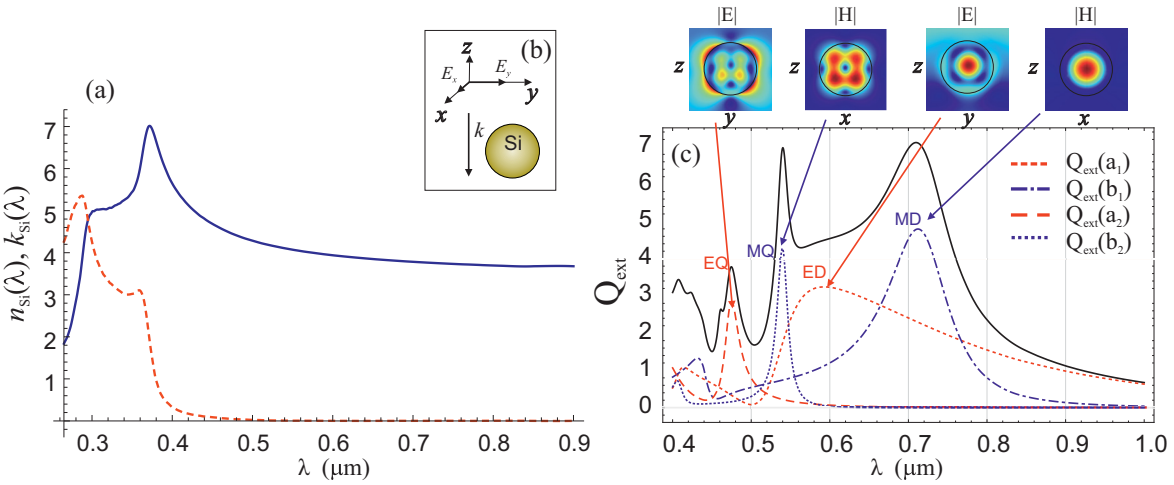

FIG. 1. (a) Refractive index (blue solid line) and extinction coefficient (red dashed line) of silicon vs wavelength [41]; (b) setting of the system; (c) normalized extinction cross section $Q_{\text{ext}} = \sigma/\pi r^2$ (black solid line) of silicon nanoparticle of 90 nm radius in free space calculated using Mie theory and corresponding contributions of the four modes: electric dipole (ED, red dotted line), magnetic dipole (MD, blue sashed-dotted line), electric quadrupole (EQ, red dashed line), and magnetic quadrupole (MQ, blue dotted line). Insets show the near-field spatial distribution of the electric (in yz plane) and magnetic (in xz plane) field amplitudes corresponding to the ED, EQ and MD, MQ resonances.

patterns obtained by these two approaches [Figs. 2(c) and 2(d)] are in perfect agreement. The previous analysis can also be extended for the polarization degree patterns for all four resonant wavelengths. Also, it allows 3D pattern analysis using 2D cross sections and taking into account the system symmetry.

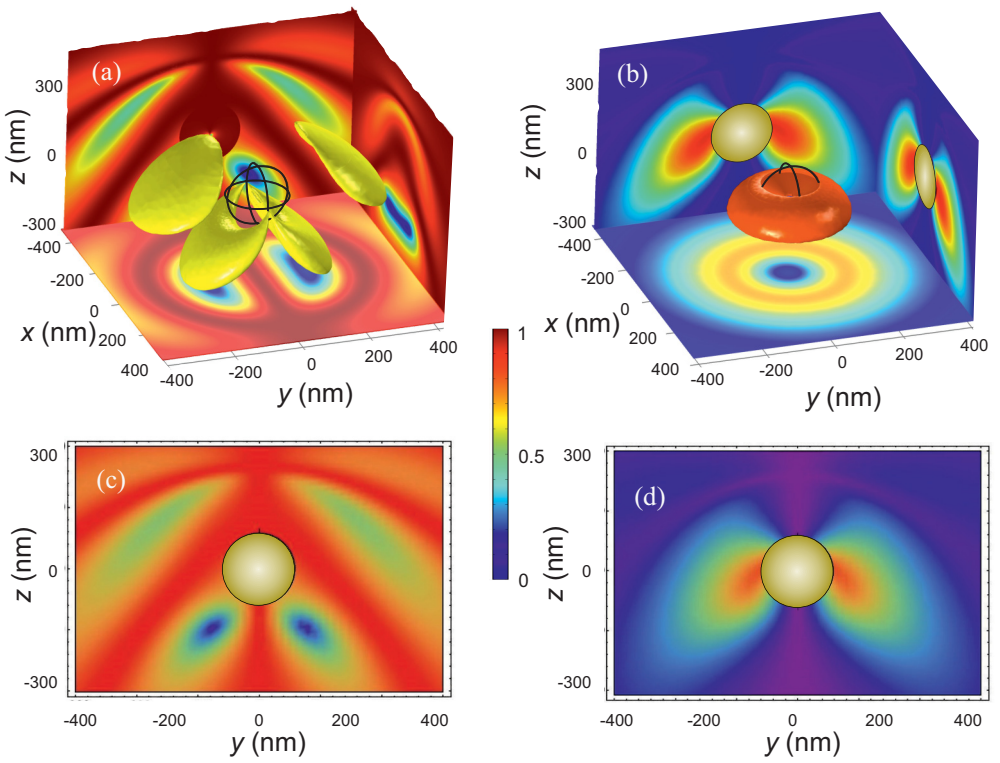

FIG. 2. Near-field polarization degree patterns calculated numerically by FEM (a), (b) and analytically (c), (d) for linear (a), (c) and circular (b), (d) polarizations of the incident light. Isosurfaces for $P = 0.6$ [yellow (a)] and $P = 0.8$ [red (b)] are shown. The origin of the coordinates coincides with the center of the nanosphere. For each of the two cases, a set of three cross sections is shown (a), (b). Each cross section shows distribution of the polarization degree in the corresponding plane: $(x, y, -180)$, $(x, 100, z)$, $(0, y, z)$ (a) and $(x, y, -90)$, $(x, 0, z)$, $(0, y, z)$ (b) for linearly and circularly polarized incident light, respectively. Note that each cross section for (a) and (b) is shown shifted to the side (bottom) plane of the graph, not in its exact place. The cross sections in (c) and (d) correspond to the $(0, y, z)$ plane.

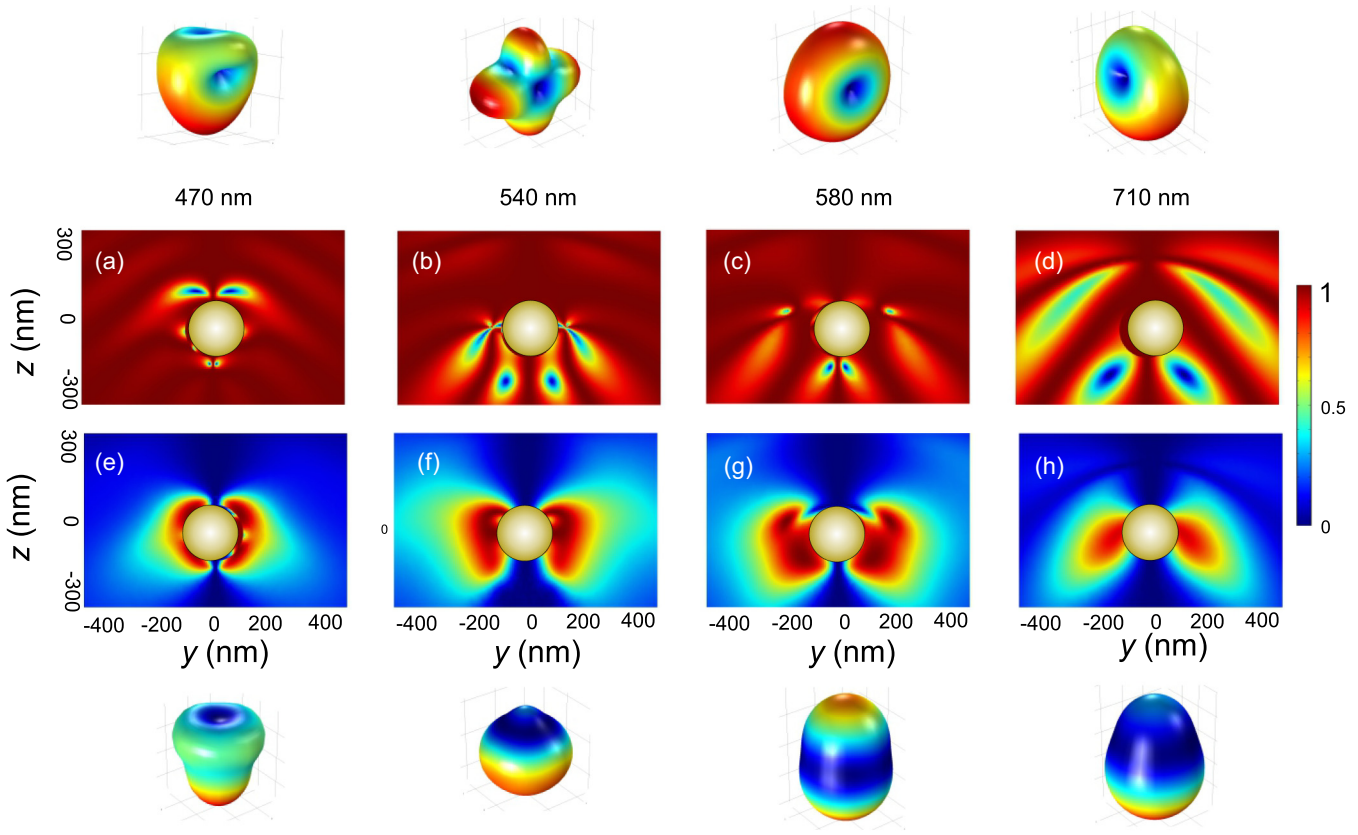

FIG. 3. Near-field polarization distributions in $(0, y, z)$ plane for the nanosphere in free space for linear (a)–(d) and circular (e)–(h) polarizations of the incident plane wave. Graphs in the columns (from left to right) correspond to the different wavelengths of the incident radiation: 470 nm (EQ mode), 540 nm (MQ mode), 580 nm (ED mode), and 710 nm (MD mode). The polarization degree P of the near field is indicated by color, where red and blue colors correspond to the linear ($P = 1$) and circular ($P = 0$) polarization, respectively. Top and bottom rows of graphs are the 3D calculated scattering diagrams for the Si nanoparticle in free space under respective polarizations of the incident field.

The yz cross sections (Fig. 3), which are most indicative, give a clear insight into the polarization degree distribution around the nanosphere. The common point for all these cases is that the polarizations of the incident field and the near field coincide at the distances of a few particle diameters and more. At the same time, in the vicinity of the nanosphere, the polarization significantly depends both on the polarization of the incident light and on its wavelength, i.e., on the type of the excited resonance.

The wavelength dependence is especially strong for the linear polarization of the incident field. For instance, the location, size, and morphology of the area in which the polarization turns to elliptical are different for different wavelengths. At $\lambda = 540$ nm [Fig. 3(b)] and $\lambda = 710$ nm [Figs. 3(d) and 2(a)] the area of strong polarization change (P decreases down to 0.5 and less) consists of four separate subareas. This corresponds to two symmetric pairs of subareas in 3D space as observed earlier in Fig. 2. By contrast, at $\lambda = 470$ nm [Fig. 3(a)] and $\lambda = 580$ nm [Fig. 3(c)] there are only two such symmetric subareas in two dimensions pointing to a single pair of subareas in 3D space. On the other hand, at $\lambda = 470$ nm the area of close-to-circular polarization is observed in the vicinity of the north pole of the nanosphere, whereas at the other three wavelengths it is mainly situated around the southern hemisphere. Also, the size of the areas is essentially affected by the wavelength. The largest area is observed for $\lambda = 710$ nm and the smallest, which is more than ten times smaller, is observed for $\lambda = 580$ nm. Altogether this shows that in the case of linear polarization of the incident light the area of elliptical polarization can be significantly transformed by choosing the mode of excitation.

In the case of circular incident polarization ($P = 0$), there also exists an area in which the polarization degree goes to 1, reaching 0.9 and even higher values, so that the polarization becomes close to linear. This area is concentrated near the equator of the nanosphere for all four resonant wavelengths [Figs. 3(e)–3(h)], corresponding to a single ring shape in 3D space. The size of the polarization switching area is significantly larger than that observed for the linear incident polarization. At the same time, the wavelength shows a noticeably weaker influence on the near-field polarization pattern. The cross sections demonstrate qualitatively similar distributions regardless of which wavelength is applied, while the effect of wavelength results in a slight change of size and cross profile of the area of polarization switch.

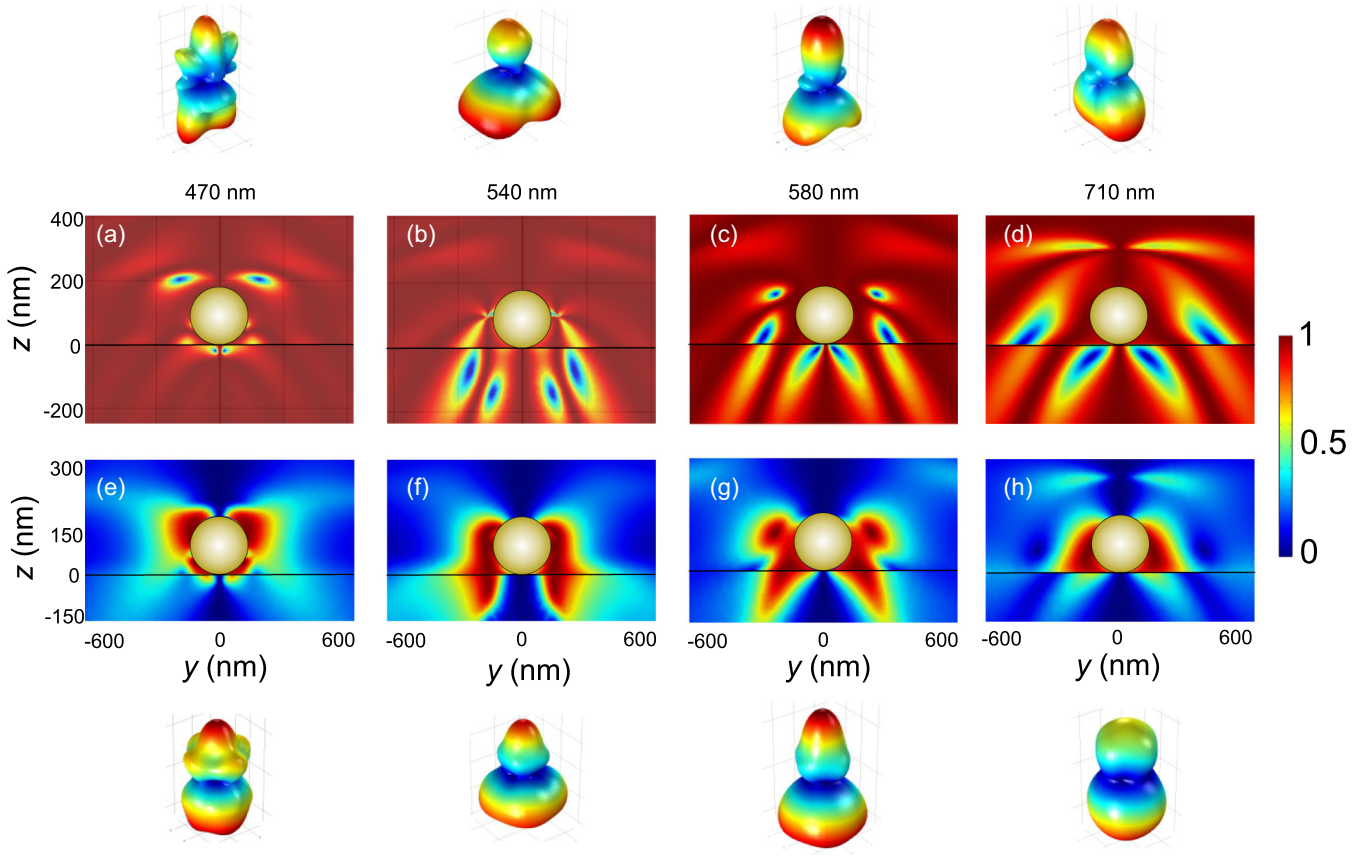

FIG. 4. Near-field polarization distribution of a Si nanosphere placed on the dielectric substrate (fused quartz) with $n = 1.5$ for the linear (top line of graphs) and circular (bottom line of graphs) polarizations of the incident light of different wavelengths: (a), (e) 470 nm (EQ mode), (b), (f) 540 nm (MQ mode), (c), (g) 580 nm (ED mode), and (d), (h) 710 nm (MD mode). Red color corresponds to the linear polarization ($P = 1$) and blue color to the circular one ($P = 0$). Top and bottom rows of graphs are the 3D calculated scattering diagrams for the Si nanoparticle placed above the dielectric substrate under respective polarizations of the incident field.

IV. NEAR-FIELD POLARIZATION PATTERN OF A DIELECTRIC NANOSPHERE NEAR A DIELECTRIC SUBSTRATE

In many applications, the nanoparticle is fixed on or located above a dielectric substrate, so that the knowledge of how the substrate affects the near field of the located nearby particle is of practical interest (see, for instance, Refs. [42–45]). Here we will assume that the nanosphere is placed upon a substrate made of fused quartz, which is often used in applications due to small absorption and monotone behavior of the dielectric constant in the optical range. The refractive index of the substrate is considered equal to 1.5 in the entire range of the wavelengths and the absorption is neglected.

We have calculated the distributions of the polarization degree in this nanoparticle-substrate system numerically using FEM and analytically (see the method described in Sec. II) and the results coincide very well, so that we present only the patterns calculated numerically. The results show that the substrate significantly affects the polarization patterns of the near field of the nanoparticle (Fig. 4). In the case of linear polarization of the incident light, the substrate causes only modest changes for the EQ resonance (at 470 nm) for which the circular polarization appears near the opposite pole of the particle. The strongest modification is observed for the wavelengths of 540 nm (MQ), 580 nm (ED), and 710 nm (MD) for which the appearing areas of circular polarization (indicated by blue) are located in the southern hemisphere. One can see also a noticeable enlargement, significant reshaping, and rearrangement of the areas, which partially penetrate into the substrate. In the case of circular polarization of the incident light, the effect of the substrate is essentially weaker. The cross profile of the single ring-shaped area of linear polarization suffers some transformation as compared to that observed in free space, but its size remains almost the same. The only qualitative difference is observed for $\lambda = 540$ nm and 580 nm at which the area of circular polarization deeply penetrates into the substrate.

These results clearly show that the polarization switches from linear to circular (or vice versa) in certain areas just above the substrate surface. The most significant effect is observed at 580 nm (ED mode) and 710 nm (MD mode) for the linear polarization of the incident light and at 540 nm (MQ mode), 580 nm (ED mode), and 710 nm (MD mode) for the circular one.

The behavior of a polarization-sensitive emitter (or a quantum scatterer) placed in such location will be different from that without the adjacent nanoparticle, which allows setting up an experiment in which interaction of the emitter with the incoming light can be switched by changing the distance

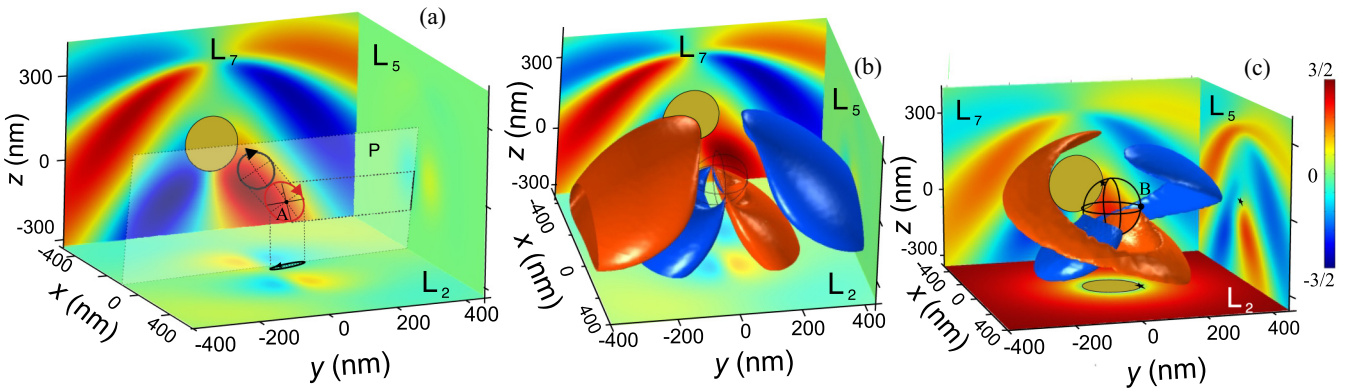

FIG. 5. Distributions of the Stokes parameters Λ_2, Λ_5, and Λ_7 in the planes $(x, y, -110)$, $(x, 100, z)$, $(-20, y, z)$ for the linear (a),(b) and $(x, y, 0)$, $(x, 90, z)$, $(0, y, z)$ for the circular (c) polarized incident light at $\lambda = 710$ nm. Polarization ellipse at point A $(-20, 100, -110)$ at which intersection of three planes is shown with the corresponding projections. Point B $(0, 90, 0)$ at which the intersection of the other three planes is also shown with the corresponding projections (indicated by stars). Red, green, and blue colors correspond to the values of $+3/2$, 0, and $-3/2$, respectively. The intermediate colors indicate elliptical polarization with the different eccentricity (see the color scale). Panels (b) and (c) show isosurfaces for the arbitrary chosen values $\Lambda_7 = \pm 0.6$ and ± 0.52, respectively.

between the dielectric nanoparticle and the emitter fixed on the substrate surface. This experiment can also be performed if the emitter is placed inside the dielectric matrix, even tens of nanometers deep under the surface. The polarization switching considered above can be performed at the wavelengths corresponding to the resonances inherent to the dielectric nanoparticle. Of practical importance is also that the resonant wavelength values can be tuned by choosing the shape or size of the nanoparticle.

V. ORIENTATION OF THE DIELECTRIC NANOSPHERE'S NEAR-FIELD POLARIZATION ELLIPSE

The distribution of the polarization degree considered above is illustrative but it does not give a complete knowledge about the polarization ellipse at each point of space in the near field. To be specific, the orientation of the polarization ellipse and the direction of electric-field vector rotation remain unspecified. Full description of the near-field polarization can be done using 3D Stokes parameters (see Sec. II), which are considered below.

Each of the Stokes parameters is a scalar field in 3D space. A clear analogy can be drawn up between some of the 3D and 2D Stokes parameters. The 3D parameter Λ_0 is analogous to the 2D parameter S_0 and describes the total spectral density of the field. The parameters Λ_2, Λ_5, and Λ_7 are analogous to S_3 and describe the eccentricity of the polarization ellipse projections to the planes xy, xz, and yz, respectively. For instance, if Λ_2, Λ_5, or Λ_7 are equal to $\pm 3/2$ (7), similar to the case of $S_3 = \pm 1$ in the 2D space, then the corresponding curve becomes a circle, and if Λ_2, Λ_5, or Λ_7 are equal to 0 then the curve degenerates into a straight line. The signs of Λ_2, Λ_5, and Λ_7 show the rotation directions for the corresponding projections: "+" and "−" correspond to the clockwise and counterclockwise directions, respectively (see an example below). The parameters Λ_1, Λ_4, and Λ_6 are analogous to the parameter S_2 and contain mixed information on both the eccentricity and orientation of the elliptical projections to the planes xy, xz, and yz, respectively. The parameter Λ_3 describing the excess of spectral density in the x direction over that in the y direction is analogous to S_1. The parameter Λ_8 represents the sum of the excesses of spectral density in the x and y directions over that in the z direction and does not have an equivalent in the case of 2D space.

According to the definitions, not each of the Stokes parameters represents a pure physical value or property that can be easily interpreted. Besides Λ_0, the most indicative are the parameters Λ_2, Λ_5, and Λ_7, so that we have calculated their distributions in the three mutually orthogonal planes for each of the two polarization types of incident radiation with $\lambda = 710$ nm. The obtained cross sections demonstrate complicated landscapes (Fig. 5), which resemble those obtained for the polarization degree shown in Figs. 2 and 3. For the linearly polarized incident field, the three arbitrary chosen planes are $(x, y, -110)$, $(x, 100, z)$, and $(-20, y, z)$ [Fig. 5(a)]. The distributions of Λ_2, Λ_5 and Λ_2, Λ_7 are found to be antisymmetrical relative to the planes $(0, y, z)$ and $(x, 0, z)$, respectively. This reflects the fact that the polarization ellipses are distributed symmetrically relative to these planes, but the rotation directions are opposite. Obtained antisymmetry is not surprising because the spherical shape of the particle and the linear polarization of the incident field leads to the reflection symmetry relative to both of the planes. The parameter Λ_7 almost reaches $\pm 3/2$ in some areas of the corresponding cross section, whereas Λ_2 and Λ_5 show relatively small deviation from zero. Moreover, the 3D isosurfaces calculated for Λ_7 [Fig. 5(b)] show a similar landscape to that obtained for the near-field polarization degree [Fig. 2(a)]. Thus, the plane in which the near-circular polarization is achieved near the nanosphere is close to the yz plane, i.e., to the polarization plane. The areas in which $\Lambda_7 \sim \pm 3/2$ correspond to the interior area of the 3D isosurfaces [Fig. 2(a)] and to the green and blue 2D areas in the linked cross sections [Figs. 2(a), 2(c) and 3(d)].

The three cross sections provide complete information about the degree of ellipticity and the rotation direction at the point of intersection A $(-20, 100, -110)$. At this point,

Λ_5 is close to zero (green color), which corresponds to the degenerative case in which the end point of the electric vector describes not an ellipse but a straight line on the plane $(x, 100, z)$. Therefore, the plane Π containing the polarization ellipse at point A is almost orthogonal to the xz plane. The parameters $\Lambda_2 \sim -0.1$ (light blue color) and $\Lambda_7 \sim 0.8$ (red color) indicate that both corresponding projections are elliptical, and the former one is strongly elongated. The rotation directions of the electric vector end point in the xy plane and the yz plane, being defined by the sign of Λ_2 and Λ_7, respectively, are counterclockwise and clockwise, respectively. Thus, the presented consideration shows how the degree of ellipticity and the rotation direction can be described and visualized at each point of space using Λ_2, Λ_5, and Λ_7. At the same time, the orientations of the projections of the polarization ellipse are encoded in Λ_1, Λ_4, and Λ_6. However, these parameters describe an interplay between the orientation and eccentricity making their visualization quite undescriptive.

For the circularly polarized incident light, a qualitative difference relates to the symmetry of 3D patterns of Λ_5 and Λ_7. According to the circular symmetry, the distributions of Λ_5 and Λ_7 are antisymmetric relative to the z axis in this case. For instance, it can be illustrated for 3D isosurfaces calculated for Λ_7 [Figs. 5(b) and 5(c)] demonstrating curved shapes which are antisymmetrically twisted around the z axis. To visualize how a near-linear polarization appears in the vicinity of the particle, the cross sections are calculated for the planes $(x, y, 0)$, $(x, 90, z)$, $(0, y, z)$ for which the point of intersection B lies on the particle's equator [Fig. 5(c)]. The parameter Λ_2 significantly deviates from the unity only in a ringlike area near the equator. Moreover, it becomes close to zero in the vicinity of the particle pointing to near-linear projection of the polarization ellipse on the xy plane. The parameter Λ_5 is also found to be close to zero near point B. At the same time, Λ_7 shows gradient behavior in the vicinity of point B, however it also achieves near-zero values not far from it. As a result, in the vicinity of point B there appears an area that is characterized by strongly elongated elliptical projections of the polarization ellipse on all the three orthogonal planes. This corresponds to near-linear polarization appearing near the equator of the particle in accordance with the patterns obtained for the polarization degree [Figs. 2(b), 2(d), and 3(h)].

VI. CONCLUSIONS

In this work, we have analyzed the polarization patterns in the vicinity of a high-refractive-index dielectric nanosphere both in free space and placed above a dielectric substrate for the linearly and circularly polarized incident light. Four wavelengths that are in resonance with ED, EQ, MD, and MQ modes of the nanoparticle have been taken into consideration. Obtained patterns have been visualized by mapping the polarization degree and the 3D Stokes parameters. The

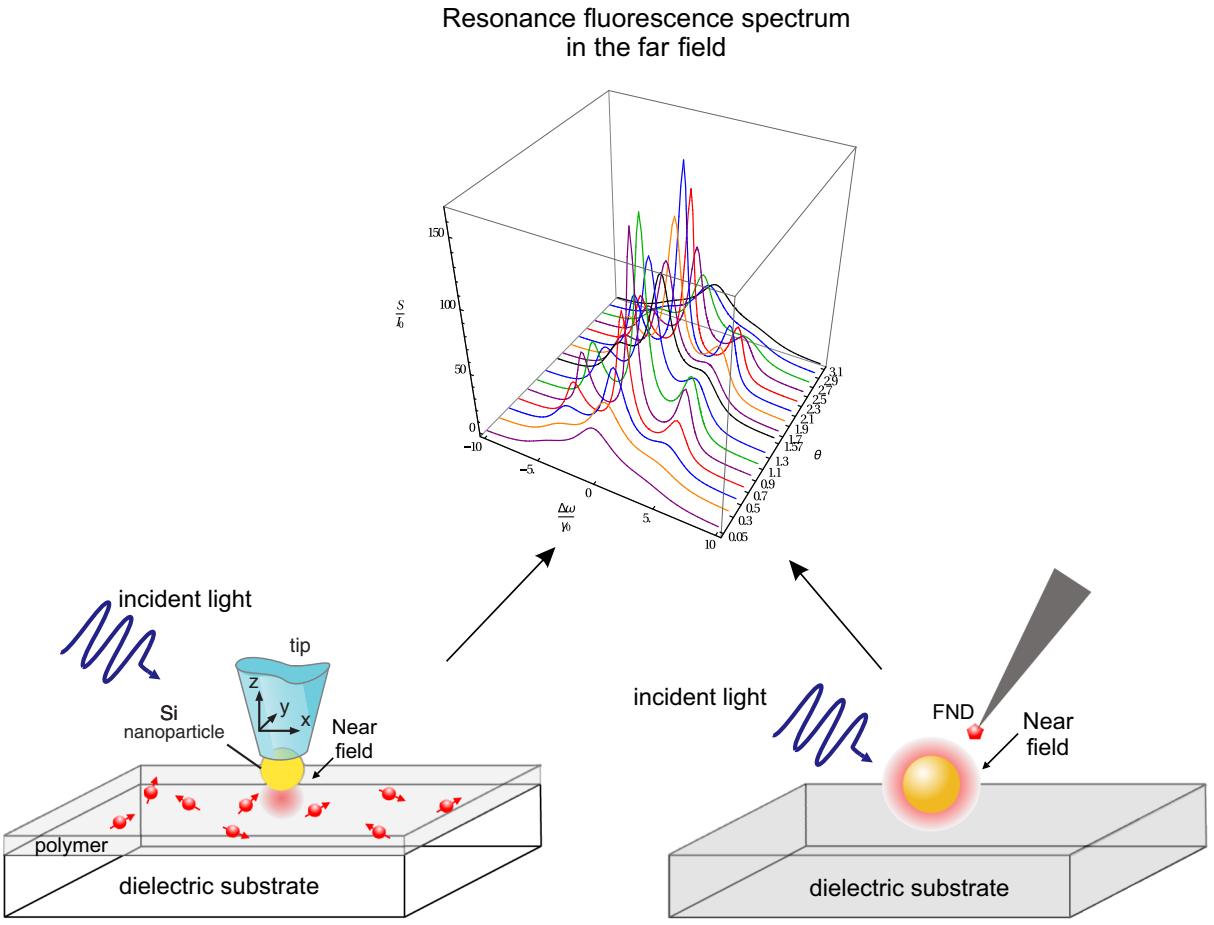

FIG. 6. Schemes of two potential experiments to map the near-field intensity and polarization around the nanoparticle.

analysis shows that the polarization is drastically affected by the nanosphere leading to a complicated structure of the near field: linear polarization of the incident light results in circular polarization (and vice versa) in certain areas in the vicinity of the nanosphere. In the presence of a dielectric substrate, the areas of polarization switch shift to other locations, change in size, and in some cases penetrate under the substrate surface. The sizes of these areas are found to be dependent on both the resonance mode excited and the incident polarization. However, in any case the size appears to be much larger than a single emitter, encouraging experimental examination. The results obtained underline the importance of taking into account the polarization distribution around the particle when considering the interaction between the emitter and the near field, which is of great importance for applications. The consideration presented here can be extended to a system consisting of any nonmagnetic and nonabsorbing medium filling the space around the dielectric nanoparticle of any shape placed near a dielectric substrate.

Potential experiments to map the near-field intensity and polarization one could think about are schematically shown in Fig. 6. In one of them (Fig. 6, left), the near-field around the nanoparticle can be measured by a quantum emitter (a fluorescent molecule or a quantum dot) embedded into a polymer film deposited on a dielectric substrate. The nanoparticle itself is attached to the tip, which can be precisely positioned in the close vicinity of the emitter. This system nanoparticle + emitter is excited by an incident laser light with the required polarization [44,45]. One can measure then the resonance fluorescence spectrum of the emitter in the far field, which gives information on both the intensity and polarization of the near field in the point of space the emitter is located [31].

Alternatively, the experiment can be done with a dielectric nanoparticle deposited above or on the dielectric substrate, which can easily be done experimentally [42,43]. A quantum emitter [for example, a fluorescent nanodiamond (FND) with *NV* center] can be embedded on a tip, which can be positioned around the nanoparticle with high precision [46]. The spectrum of resonance fluorescence of this emitter measured in the far field will give then a detailed information about the intensity and polarization of the near field in the point the emitter is located.

Another, different experimental strategy for 3D polarization mapping is the following: A nanoparticle is placed in a viscous liquid containing fluorescent molecules, which slowly descend due to gravitation. The molecules, moving down around the particle, are used as emitters in one of polarization-sensitive schemes with application of single-molecule spectromicroscopy that allows precise spatial detection of the molecule [47].

ACKNOWLEDGMENT

The authors would like to acknowledge financial support from the Russian Foundation for Basic Research under Grant No. 18-52-53040.

[1] B. Hecht and L. Novotny, *Principles of Nano-Optics* (Cambridge University Press, Cambridge, UK, 2006).
[2] V. V. Klimov, *Nanoplasmonics* (Pan Stanford, Singapore, 2014).
[3] M. Decker and I. Staude, J. Opt. **18**, 103001 (2016).
[4] M. Stockman, Opt. Express **19**, 22029 (2011).
[5] A. I. Kuznetsov, A. E. Miroshnichenko, M. L. Brongersma, Yu. S. Kivshar, and B. Luk'yanchuk, Science **354**, aag2472 (2016).
[6] A. E. Krasnok, A. E. Miroshnichenko, P. A. Belov, and Y. S. Kivshar, Opt. Express **20**, 20599 (2012).
[7] E. M. Purcell, Phys. Rev. **69**, 37 (1946).
[8] O. L. Muskens, V. Giannini, J. A. Sánchez-Gil, and J. G. Rivas, Nano Lett. **7**, 2871 (2007).
[9] J. N. Farahani, D. W. Pohl, H. J. Eisler, and B. Hecht, Phys. Rev. Lett. **95**, 017402 (2005).
[10] P. J. Schuck, D. P. Fromm, A. Sundaramurthy, G. S. Kino, and W. E. Moerner, Phys. Rev. Lett. **94**, 017402 (2005).
[11] T. H. Taminiau, R. J. Moerland, F. B. Segerink, L. Kuipers, and N. F. van Hulst, Nano Lett. **7**, 28 (2007).
[12] E. D. Chubchev, Yu. V. Vladimirova, and V. N. Zadkov, Opt. Express **22**, 20432 (2014).
[13] E. D. Chubchev, Yu. V. Vladimirova, and V. N. Zadkov, Laser Phys. Lett. **12**, 015302 (2015).
[14] Yu. V. Vladimirova, A. A. Pavlov, and V. N. Zadkov, Moscow Univ. Phys. Bull. **72**, 544 (2017).
[15] K. S. Grigoriev, N. Yu. Kuznetsov, Yu. V. Vladimirova, and V. A. Makarov, Phys. Rev. A **98**, 063805 (2018).
[16] P. Biagioni, M. Savoini, J.-S. Huang, L. Duo, M. Finazzi, and B. Hecht, Phys. Rev. B **80**, 153409 (2009).
[17] R. Mohammadi, A. Unger, H. J. Elmers, G. Schönhense, M. Z. Shushtari, and M. Kreiter, Appl. Phys. B **104**, 65 (2011).
[18] M. Celebrano, P. Kukura, A. Renn, and V. Sandoghdar, Nat. Photon. **5**, 95 (2011)
[19] E. S. Arinze, B. Qui, G. Nyirjesy, and S. M. Then, ACS Photon. **3**, 158 (2016).
[20] D. W. Pohl and D. Courjon, *Near-Field Optics*, NATO Advanced Scientific Institutes Series E242 (Springer, Dordrecht, 1993).
[21] D.-S. Kim and Z. H. Kim, Opt. Express **20**, 8689 (2012).
[22] S. S. Kharintsev, A. R. Gazizov, M. Kh. Salakhova, and S. G. Kazarian, Phys. Chem. Chem. Phys. **20**, 24088 (2018).
[23] S. S. Kharintsev, A. I. Fishman, S. G. Kazarian, and M. Kh. Salakhov, Phys. Rev. B **92**, 115113 (2015).
[24] T. Mino, Y. Saito, and P. Verma, Appl. Phys. Lett. **109**, 041105 (2016).
[25] K. D. Parky and M. B. Raschke, ACS Nano Lett. **18**, 2912 (2018).
[26] B. Rolly, B. Stout, and N. Bonod, Opt. Express **20**, 20376 (2012).
[27] P. Albella, M. A. Poyli, M. K. Schmidt, S. A. Maier, F. Moreno, J. J. Saénz, and J. Aizpurua, J. Phys. Chem. C **117**, 13573 (2013).
[28] B. S. Luk'yanchuk, N. V. Voshchinnikov, R. Paniagua-Dominguez, and A. I. Kuznetsov, ACS Photon. **2**, 993 (2015).
[29] M. I. Tribelsky, J. M. Geffrin, A. Litman, Ch. Eyraud, and F. Moreno, Sci. Rep. **5**, 122288 (2015).
[30] Yu. V. Vladimirova, E. D. Chubchev, and V. N. Zadkov, Laser Phys. **27**, 025901 (2017).

[31] Yu. V. Vladimirova, V. V. Klimov, V. M. Pastukhov, and V. N. Zadkov, Phys. Rev. A **85**, 053408 (2012).
[32] G. Mie, Ann. Phys. **330**, 377 (1908).
[33] P. Debye, Ann. Phys. **335**, 57 (1909).
[34] H. Weyl, Ann. Phys. **364**, 101 (1919).
[35] A. J. Devaney and E. Wolf, J. Math. Phys. **15**, 234 (1974).
[36] P. A. Bobbert and J. Vlieger, Physica A **137**, 209 (1986).
[37] P. A. Bobbert, J. Vlieger, and R. Greef, Physica A **137**, 243 (1986).
[38] M. Born and E. Wolf, *Principles of Optics: Electromagnetic Theory of Propagation, Interference and Diffraction of Light* (Cambridge University Press, Cambridge, UK, 2000).
[39] B. S. Lukyanchuk, Y. W. Zheng, and Y. F. Lu, Laser cleaning of solid surface: optical resonance and near-field effects, in *Proceeding of SPIE*, Vol. 4065 (SPIE, 2000).
[40] T. Setälä, A. Shevchenko, M. Kaivola, and A. T. Friberg, Phys. Rev. E **66**, 016615 (2002).
[41] G. Vuye, S. Fisson, V. Nguyen, V. Y. Wang, J. Rivory, and F. Abelés, Thin Solid Films **233**, 166 (1993).
[42] V. Valuckas, R. Paniagua-Dominguez, Y. H. Fu, B. Luk'yanchuk, and A. I. Kuznetsov, Appl. Phys. Lett. **110**, 091108 (2017).
[43] X. Zhang, Yi. Xu, J. Liu, J. Li, J. Xiang, H. Li, J. Li, Q. Dai, S. Lan, and A. E. Miroshnichenko, Nat. Commun. **9**, 2964 (2018).
[44] P. Anger, P. Bharadwaj, and L. Novotny, Phys. Rev. Lett. **96**, 113002 (2006).
[45] S. Kühn, U. Håkanson, L. Rogobete, and V. Sandoghdar, Phys. Rev. Lett. **97**, 017402 (2006).
[46] I. V. Fedotov, N. A. Safronov, Yu. A. Shandarov, A. A. Lanin, A. B. Fedotov, S. Ya. Kilin, K. Sakoda, M. O. Scully, and A. M. Zheltikov, Appl. Phys. Lett. **101**, 031106 (2012).
[47] P. J. S. Smith, I. Davis, C. G. Galbraith, and A. Stemmer, J. Opt. **15**, 090201 (2013).